2008 20th International Lightning Detection Conference
21-23 April • Tucson, Arizona, USA
2nd International Lightning Meteorology Conference
24-25 April • Tucson, Arizona, USA

MODELING AND CALIBRATION OF VAISALA'S OPERATIONAL LONG RANGE LIGHTNING DETECTION NETWORK

Kenneth L. Cummins
Department of Atmospheric Sciences, University of Arizona
Tucson, AZ, USA

Martin Murphy, Nick Demetriades, Burt Pifer
Vaisala Inc.
Tucson, AZ, USA

Antti Pessi, Steven Businger
University of Hawaii

1. INTRODUCTION

Lightning detection has great value for real-time storm tracking, warning, and nowcasting (e.g. Johnson et al. 1982; Demetriades and Holle 2005; Squires and Businger 2008). In remote regions where conventional data sources are not available, tracking of thunderstorms and assessing cyclone intensification are important challenges in weather prediction. Lightning is one of the few meteorological phenomena that can be continuously observed in both space and time in these remote regions, because of the long-range propagation characteristics of lightning electromagnetic fields in the VLF frequency range. By virtue of the relationship between lightning and rainfall rates, these data also hold promise as input for Numerical Weather Prediction (NWP) models as a proxy for latent heat release in convection.

In this paper, we evaluate the instrumentation currently employed in Vaisala's Long Range Lightning Detection Network (LLDN). Furthermore, we describe the development of detection efficiency (DE) and location accuracy (LA) models and derive model parameters used to create model estimates of LA and DE over the operating domain of Vaisala's operational LLDN.

2. BACKGROUND

The large electromagnetic signals associated with return strokes in cloud-to-ground (CG) and very large pulses in cloud discharges are mainly observable in the low frequency (LF) and very low frequency (VLF) regions of the spectrum (Cummins et al. 1998a). When propagation distances are less than about one thousand km, significant energy in both the VLF and LF band can propagate as a ground wave, as shown in Fig. 1. At greater distances, energy in the VLF portion of the spectrum between 3 and 30 kHz (Sferics) can propagate effectively in the waveguide defined by the earth's surface below and by the ionosphere above, specifically its lowest layer, the D region. Out to propagation distances of roughly 4000 km, most of the energy is carried in signals that can be accounted for using the first two "ionospheric hops" shown in Fig. 1. At even greater distances, propagation is more-efficiently characterized using modal analysis (Wait, 1968).

Waveforms associated with ionospherically reflected fields are quite different than typical ground waves produced by CG lightning return strokes (Fig. 2). Note the sharp initial downward peak and short peak-to-zero time for the ground wave at 264 km (Fig. 2a). At a distance of 860 km, Fig. 2b shows a distinct initial downward ground wave followed by a single-hop ionospheric reflection of opposite polarity (Kelso, 1964). At a distance of 3400 km (Fig. 2c), the waveform is determined by multiple ionospheric components, but there is evidence of a very small initial downward ground wave, a slightly larger first-hop (inverted) sky wave, and a larger downward second-hop sky wave (at ~450 μS). Although this distant signal contains clear sky-hop components, its overall waveform would be best-described using mode theory. Since the field produced by a return stroke generally changes polarity at each reflection, the original polarity of the reflected waves cannot be readily determined, unless the ground wave is clearly identifiable.

Propagation characteristics of the ionosphere differ between night and day, due to

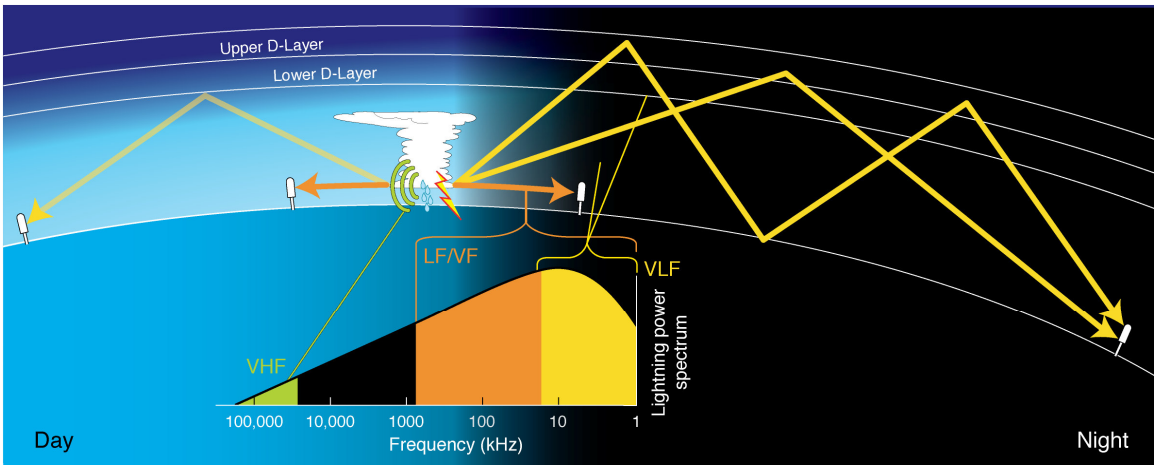

Figure 1 Schematic diagram of the Earth-ionosphere wave-guide, which allows VLF (3-30 kHz) emissions from thunderstorms (sferics) to propagate thousands of kilometers through reflection. The best propagation is observed over the ocean at night.

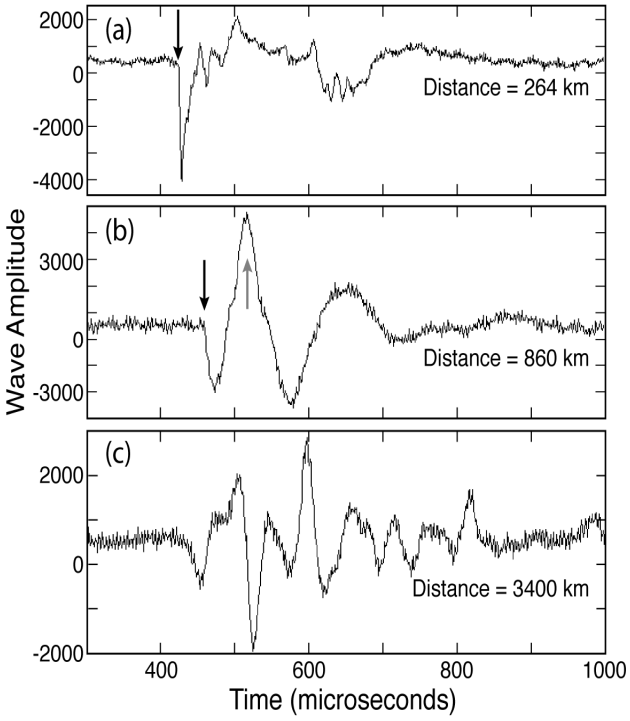

Figure 2. Vertical electric field waveforms for a cloud-to-ground return stroke detected by sensors located at 264, 860, and 3400 km from the lightning stroke. The amplitude scale is uncalibrated. Black arrows in a) and b) indicate initial appearance of the ground wave, and the gray arrow in b) indicates the single-hop reflected wave.

variations in the electron densities. Electron densities increase rapidly with height in the D region, typically from a few per cm^3 to a few hundred per cm^3. VLF waves typically reflect from the heights 60-75 km during the daytime when high electron densities extend into the lower ionosphere. During the night the high electron density retreats to higher altitudes, with the reflections occurring in the range 75-90 km.

Ionospheric D region characteristics are often defined by two parameters, the reflection height and exponential sharpness factor (rate of increase of electron density with height - (Wait and Spies 1964)). These parameter values are particularly stable during the day, resulting in predictable daytime wave propagation (Thomson 1993; McRae and Thomson 2000). The characteristics of the nighttime ionosphere are more variable and the signal propagation is less predictable than by day.

It is commonly known that eastward and westward propagating VLF waves have different propagation characteristics (e.g. Taylor 1960). The mean attenuation rate for subionospheric, westward propagating waves have been observed to be somewhat greater than for eastward propagation. Nickolaenko (1995) used a VLF navigation system Omega at 10.2 kHz in the Atlantic and found attenuation rates of 2.1

dB Mm^{-1} for eastward propagation and 2.6 dB Mm^{-1} for westward propagation.

The somewhat simplified approach taken in this paper will be to employ different model parameters for daytime and nighttime propagation that take into account diurnal changes in ionospheric electron density, as well as ocean-vs-land differences in ground conductivity, but that ignore directional propagation effects. Measurements presented in Section 2 support this approach. Since the propagation distances of interest are at or below 4000 km, analysis and results will be presented in terms of ground-wave and sky-hop propagation, rather than the more-complete modal analysis that is required at longer propagation distances.

Vaisala's approach to long range lightning detection is somewhat different than what is employed by other longer range detection systems (Rodger et al. 2006, Chronis and Anagnostou 2003, Nash et al. 2005, Keogh et al. 2006). Vaisala's LLDN location algorithm employs time-of-arrival (TOA) coupled with magnetic direction finding (MDF), which allows lightning discharges to be located using as few as two sensors. The network employs a subset of the ~200 broadband (VLF/LF) sensors from the U.S. National Lightning Detection Network (NLDN) and the Canadian Lightning Detection Network (CLDN), as well four VLF "PacNet" sensors located in Hawaii, Kwajalein, and Alaska. The broadband LF/VLF sensors in the NLDN and CLDN are not optimized for long range detection, but still provide important contributions to the overall network performance. The VLF PacNet sensors are operationally equivalent to the NLDN sensors, but have a narrower bandwidth and are operated at higher gain.

A particularly salient difference is that Vaisala's system also employs knowledge of the mixed ground and ionospheric propagation characteristics for distances less than about 4000 km. This knowledge is used to specifically identify the signals reported by self-consistent groups of sensors experiencing similar propagation paths (see Section 2). This results in good location accuracy (better than 10 km median error) at distances of 2000-3000 km from the U.S/Canada borders. Performance at greater distances varies with network geometry, including the influence of the PacNet sensors in the central Pacific region.

3. SENSOR EVALUATION

Basic sensor characteristics have been determined using data from a PacNet test sensor located in Tucson, Arizona, collected in 2002. These data were compared to NLDN data collected during a specific week in which a strong midlatitude storm system with attendant squall-lines propagated from the High Plains across to the East Coast, providing robust lightning strike data with propagation distances ranging between 100 and 4000 km.

In this section, we parameterize the propagation effects in terms of signal attenuation and propagation delay. We show that the type of propagation (ground wave, first hop, and second hop) can be deduced from polarity inversions and arrival time delay. Azimuth and timing deviations are also measured, to be used in location accuracy modeling (Section 4).

3.1 Effects of Propagation

As discussed in section 1, long range propagation of lightning "sferics" involves a complex interaction between the earth and the ionosphere. The behavior of this propagation medium varies with time-of-day, conductivity of the earth path, and (to a lesser degree) season and direction. Since we are primarily interested in a "first order" characterization of propagation over salt water, it is reasonable to simply partition propagation into two conditions: day and night. It has been shown that propagation characteristics between two widely separated locations (both attenuation and phase (delay) changes as a function of frequency) transition fairly continuously from the daytime behavior to the nighttime behavior, over a period of 2-3 hours.

The propagation characteristic that directly affects peak signal strength is the amplitude attenuation as a function of frequency and distance. This can be approximated by the expression

$$Att = \frac{\alpha}{R}\sqrt{\left(\frac{\theta}{\sin(\theta)}\right)}\exp\left(-\frac{R}{\lambda}\right) \qquad (1)$$

Where α is a scaling constant, R is the distance along the earth surface between the lightning discharge and a remote sensor, $\theta = \frac{R}{R_e}$, and R_e is the radius of the earth (Al'pert, 1963). The attenuation rate (1/λ) is the inverse of the e-folding distance (the distance at which propagation losses reach 1/e), and is primarily dependent on the conductivity of the earth-portion of the path and the electron density profile in the atmosphere. This expression is a simplification of the general propagation models described by Wait (1968) and others, but empirical evidence suggests that it captures the average behavior of broadband sferics over modest propagation distances (<4000 km).

The attenuation rate for the test sensor was evaluated by time-correlating its data with NLDN data collected throughout the U.S., and comparing the lossless signal strength (determined by the NLDN estimated peak current and the known distance) with the peak field strength measured by the test sensor.

The analysis of signal strength shows the expected exponential loss in energy with distance (Fig. 3), where the average relative field strength (filled circles) is normalized by the estimated NLDN peak current. The standard deviation error bars show larger errors in the range of 2000-3500 km, where propagation involves a mix of ground and ionospheric propagation (see section 3.3, Fig. 6). The daytime e-folding distance shown in Fig. 3a is 10,000 km, and the nighttime e-folding distance is 40,000 km (Fig. 3b).

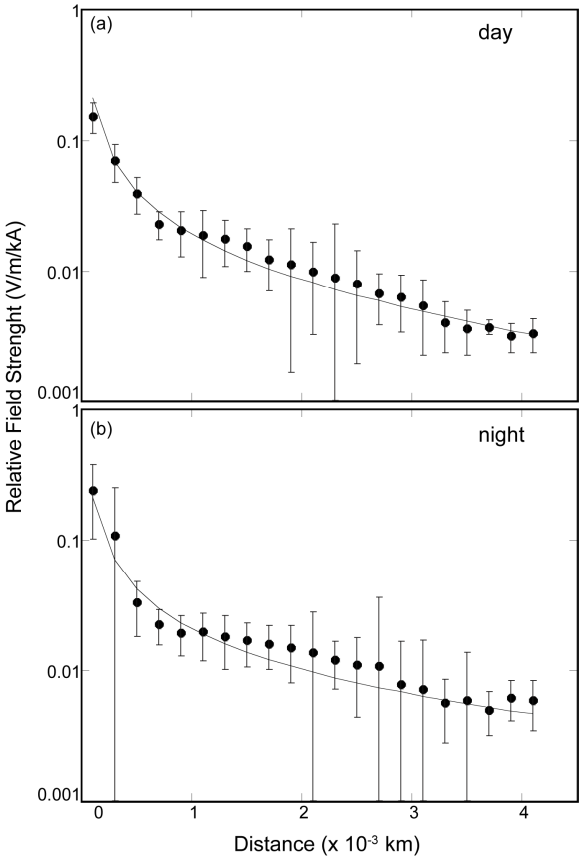

Figure 3. Relative signal strength as a function of stroke distance as detected by a test sensor located in Tucson, Arizona for (a) day and (b) night. The error bars are ±1 standard deviation.

3.2 Timing and Angle Errors

Timing errors were calculated by time-correlating data from the PacNet test sensor with NLDN data and comparing speed-of-light propagation time (determined from the NLDN stroke time and the known propagation distance) with the arrival time measured by the sensor (Fig. 4). These histograms show the time differences measured with an accuracy of approximately one μs. All reports from one week of observations are included in this analysis.

Figs. 4a and c include reports with the same polarity as the NLDN peak current, and Figs. 4b and d include opposite-polarity reports. The polarity reversal (relative to the polarity determined by the NLDN) occurs when the earlier signal components (ground wave, then 1st-hop, then 2nd-hop) fall below the fixed detection threshold of the sensor.

The ground wave signal delay distributions (mean and standard deviation (σ)) were nearly the same for day and night (mean=20.0 μs, σ=5.0 μs and mean=19.3 μs, σ=4.7 μs, respectively, Figs. 4a, c). The first-hop sky-wave distribution shifted from a daytime mean value of 52.9 μs (σ=4.7 μs) to night value of 70.5μs (σ=4.0 μs, Figs. 4b, d). The second-hop distribution shifted from a daytime mean value of 90.0 μs (σ=5.1 μs) to night value of 104.0 μs (σ=8.0 μs, Figs. 4a, c). Note that the polarity

reversal of the first hop helps distinguish it from the ground-wave and second-hop signals, and that the signal delay distributions have almost no temporal overlap.

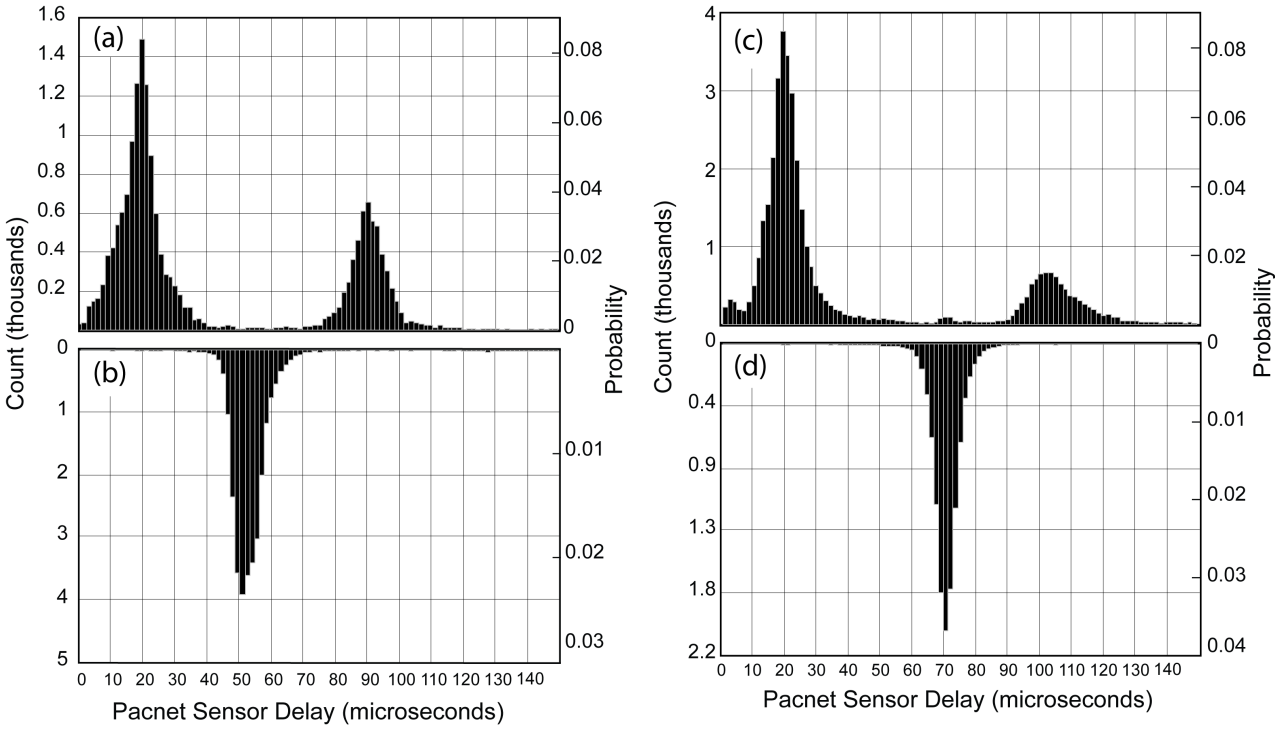

Figure 4. (a) Daytime ground wave signal delay distribution is centered at 20.0 μs and has a standard deviation of 5.0 μs. Second-hop sky wave distribution is centered at 90.0 μs (σ=5.1 μs). (b) First-hop (inverted) sky-wave distribution is centered at 52.9 μs and has a standard deviation of 4.7 μs (graph inverted in reference to reversed polarity of first hop). (c) Night-time average for ground-wave distribution is 19.3 μS (σ=4.7 μS). Second-hop wave 104.0 μS, with σ=8.0 μS. (d) First-hop distribution is centered at 70.5 μS with σ=4.0 μS (graph inverted in reference to reversed polarity of first hop).

Angle errors were calculated by time-correlating data from the test sensor with NLDN data (150 μs time window) and comparing the true azimuth from the sensor (determined from the NLDN stroke location) with the azimuth measured by the sensor. An angle error histogram was derived from all time-correlated events with signal strengths from just above threshold to four times threshold (Fig. 5). The parametric fit has a mean value of -4 degrees (resulting from an uncorrected antenna rotation and site errors due to local site conditions), and a standard deviation of 4.5 degrees. This value is conservative since it includes polarization errors and the (correctable) variation of the local site error around its mean value.

3.3 Identification of Propagation Mode

The distinct separation of timing between ground-, first-hop-, and second-hop waves can be used to identify the wave type, as illustrated in Fig. 6. Within ~500 km of the sensor, nearly 100% of the signals are ground waves. Beyond that, the percentage of the first-hop waves increases sharply, whereas the ground wave percentage decreases. They become equal at 900-1000 km. As noted earlier, the error bars for the observations of relative signal strength with distance are greatest at distances where there is significant overlap in the wave types (compare Figs. 6 and 3).

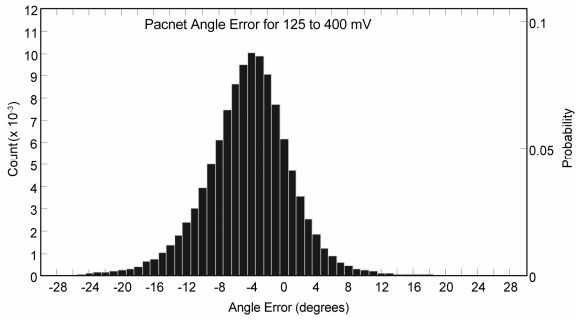

Figure 5. Angle error without site-error correction has a mean value of -4.0 degrees and a standard deviation of 4.5 degrees (for both day and night).

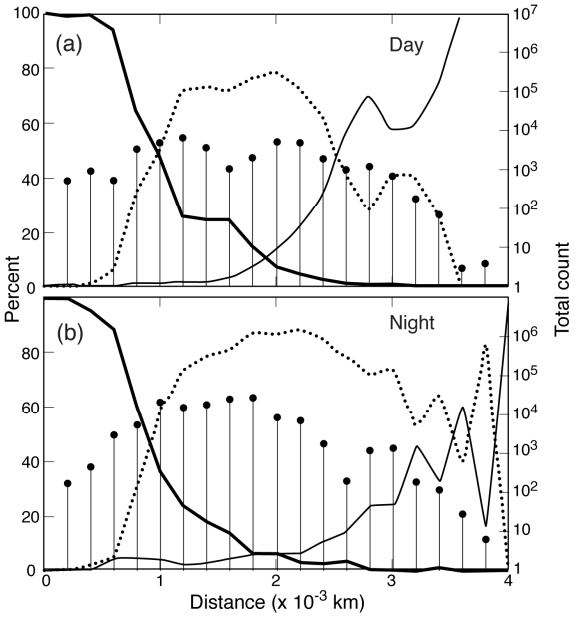

Figure 6. Percentage of different propagation types as a function of distance for (a) day and (b) night. Dark solid line is for ground wave, dotted for first-hop sky-wave, and thin solid for second-hop sky-wave. The bars indicate the total number of strikes detected in each 200 km distance bin (right ordinate).

4. MODELING AND CALIBRATION

Quantitative applications of lightning information require knowledge of the detection efficiency (DE) and location accuracy (LA) of the network. Models can be used to estimate these parameters throughout the domain of the network. In this section, we discuss the modeling process and then we construct specific model estimates of DE and LA using sensor parameters from Section 3 and "ground-truth" data obtained from a short-baseline lightning location system (LLS) in Puerto Rico.

As discussed in the Appendix, there are numerous factors that determine the DE of an LLS. To summarize, the fundamental information required to accurately model network DE is the distribution of peak currents, the detection threshold characteristics of the sensors, the propagation conditions (regional conductivity and ionospheric conditions) and knowledge of the location method (2, 3, or 4 sensors required to get a location). The detection threshold characteristics of the sensor are strictly a function of the incident peak field strength and the gain and threshold of the sensor. The characteristics have been determined in a laboratory setting and confirmed in field tests of performance by Vaisala. The location method employed in this network is the IMPACT method which combines time-of-arrival and direction finding, so a minimum of two sensors are required to detect a stroke so it can be reported by the network.

4.1 Peak current distribution for salt-water path

The form of the propagation model provided in Eq. 1 was shown to be a reasonable approximation of the observations from NLDN and a PacNet test sensor located in Arizona (see Fig. 3). To estimate DE for the LLDN, the two remaining parameters (peak current distribution and propagation characteristics; i.e., e-folding distances) are needed for salt-water path conditions. These parameters were obtained by comparing recent information produced by the LLS operated by the Puerto Rico Electric Power Authority (PREPA) with information produced by the LLDN in the western Atlantic Ocean. The PREPA network is a short-baseline network comprised of five low-gain IMPACT sensors installed in 2003. Based on analyses performed by Vaisala, this network has a CG flash DE in excess of 95% over Puerto Rico and nearby surrounding waters, and a median location error of 500 m or less.

It has been shown (Orville and Huffines 2001) that the median peak current value for negative first strokes, inferred from LLS measurements, are somewhat larger when a stroke strikes salt water than when it strikes ground. It is unknown whether this enhancement is the result of a change in the relationship between peak field and peak current over salt water, or an actual increase in peak current in the channel. Either way, this effect produces a change in the population of "source" signals over salt water that needs to be accounted for when estimating LLS DE over the oceans.

To account for this salt-water effect, the peak current distribution was constructed using negative first strokes obtained from the PREPA LLS for the calendar year 2006 (Fig. 7), obtained from the "Sea" region surrounding Puerto Rico (Fig. 8c).

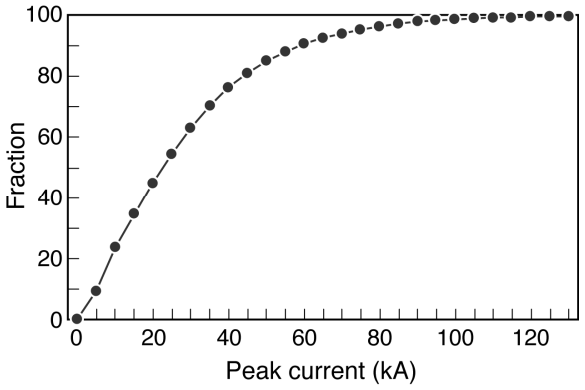

Figure 7. Cumulative peak current distribution derived from negative CG first strokes striking salt water near Puerto Rico.

4.2 Calibration of DE model

The remaining free parameters in the DE model relate to the propagation characteristics during day and night conditions. In our model, this is embodied in the e-folding distance (space constant). These parameters were estimated by adjusting the e-folding distances so that the model-estimated performance in Puerto Rico matched the measured performance derived from direct comparisons of the two networks.

For both day and night conditions, the relative flash DE of the LLDN was obtained by computing the fraction of flashes reported by the PREPA network (over the domain in Fig. 8c) that had time-correlated events reported by the LLDN (within 350 µSec of any stroke in the flash). Daytime (night-time) statistics were only computed between the hours of 12 (00) and 22 (10) UTC, when the propagation path between Puerto Rico and the LLDN sensors was all daylight (night), with no terminator crossing between Puerto Rico and LLDN sensors. LLDN DE was defined as the percentage of PREPA CG flashes detected by the LLDN. The observed flash DE values were 4.7% for day and 20.8% for night.

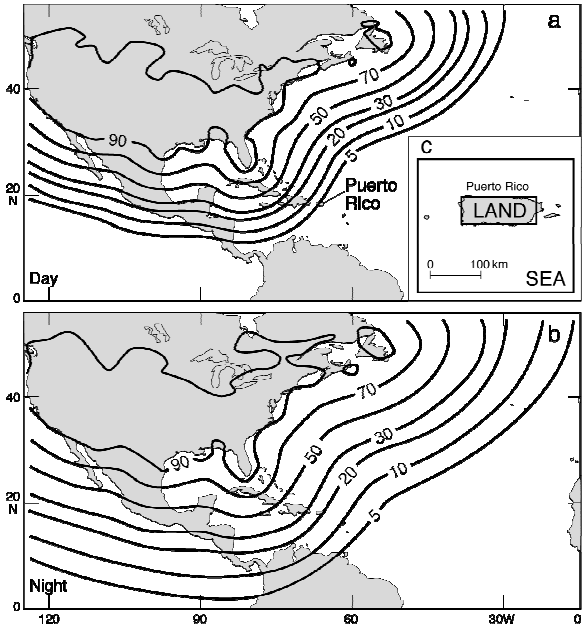

Figure 8. Results from the detection efficiency model show (a) 5% day and (b) 20% night DE over Puerto Rico when using the reference peak-current distribution and space constants of 2000 and 6000 km for day and night, respectively. (c) Insert: Lightning data analysis region for Puerto Rico. The salt-water region is the "Sea" region, with the exclusion of the "Land" region.

The e-folding distances in the DE model were adjusted (2000 km during the day and 6000km at night) so that the predicted DE (~5%

day and ~21% night) was consistent with the observed DE (Fig. 8), given the observed salt-water peak current distribution in the vicinity of Puerto Rico (Fig. 7). Note that these space constants are smaller than those observed for the PacNet test sensor, which reflects the poorer performance of the broadband (and lower gain) NLDN sensors relative to the PacNet sensor for long range detection. During the day, the DE is greater than 10% out to about 2000 km beyond the coasts of the U.S. and Canada. This extends to more than 3000 km at night. Estimated DE values below 5% are not shown because of model uncertainties.

The refined DE model was then applied to the PacNet (central Pacific) region of the LLDN, with the resulting predicted DE distribution shown in Fig. 9. In applying the refined DE model to Hawaii, it is assumed that the weather regime in the two locations, in a prevailing trade-wind belt, will produce similar peak current distributions. In this regard, it should be noted that during the period that the Puerto Rico data were analyzed, no tropical cyclones passed through the region.

The highest DE is found near the Hawaiian Islands and the U.S./Canada coastline. There is a steep gradient of DE reaching a minimum at about the halfway-point between these two high-DE areas. During the day, minimum DE in this area falls just below 10%, at a distance of about 2000 km beyond the coasts of the U.S. and Canada. This minimum increases to about 30% at night. Estimated DE falls off sharply (below 5%) to the northwest and southeast, where there are no nearby sensors.

The boxes in Figure 9 show the regions over which PacNet DE was evaluated by comparison with the NASA Lightning Imaging Sensor (LIS) on the Tropical Rainfall Measuring Mission (TRMM) satellite. The comparison between these two sensing systems involves a number of corrections that are described by Pessi et al. (2008, submitted to *Journal of Atmospheric and Oceanic Technology*). PacNet and LIS data between February 2004 and February 2007 were used for the evaluation, provided that at least 3 of the PacNet sensors were operational. For the region closer to Hawaii in Fig. 9, the LIS-relative DE was found to be 21% during the day and 57% at night. The region farther to the north of Hawaii in Fig. 9 had a LIS-relative DE of 19% during the day and 44% at night.

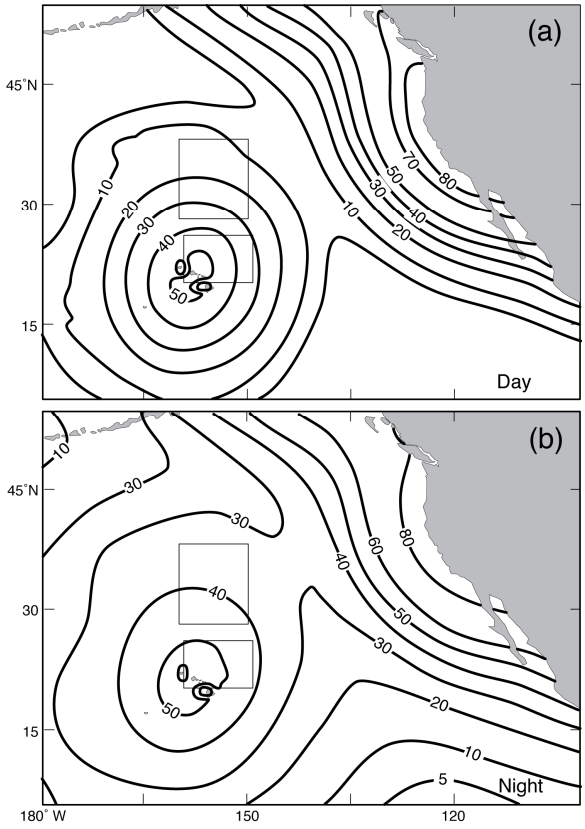

Figure 9. Modeled DE (%) over the Pacific during a) day, and b) night. The boxes show the areas where the observed DE was assessed. This stuff belongs in text with some context and discussion.

4.3 Modeling location accuracy

As described by Cummins et al. (1998b, Appendix) the median estimated location accuracy is defined as the semi-major axis of a 50th percentile location error ellipse. For the LLDN LA model, the ellipse is computed for each element of a 75x75 point grid, and is determined by sensor locations, probability of detection by specific groups of sensors (DE model), and the time and angle standard errors. The timing and angle error characteristics were derived empirically using the PacNet test-sensor data, described in section 3. These errors were parameterized as the standard deviation of normally distributed random variables (Figs. 4 and 5), resulting in a 5 μs RMS timing error value and an angle error of 4.5 degrees RMS.

The resulting modeled LA distribution in the Atlantic ranges from 1 km near the U.S. and Canadian coastline, falling off uniformly to ~30 km as the 5% DE boundary is approached (not shown). Modeled LA in the Puerto Rico area was ~16 km.

Using the same time coincidence criteria (350 µSec) mentioned in section 4.2, LLDN LA validation was performed in the Puerto Rico region using PREPA CG stroke locations as ground truth. During 2006, over 5,000 CG strokes correlated during the day and over 9,000 CG strokes correlated during the night. LLDN daytime LA was 8 km and nighttime LA was 10 km. Both of these values are slightly better than the modeled LA in the Puerto Rico area of ~16 km.

The LA in the Pacific is between ~2 and 16 km between Hawaii and North America, increasing to 64 km near the dateline over the North Pacific Ocean (Fig. 10). Areas of poor LA occur to the northwest and southeast of Hawaii, which lie on the extension of the baseline between the two Hawaii sensors. The modeled LA for the area to the southeast of Hawaii is especially large due to the absence of additional sensors in that direction. The Unalaska and Kwajalein sensors improve performance slightly to the northwest of Hawaii.

The boxes in Figure 10 show the regions over which PacNet LA was evaluated by comparison with the NASA LIS on the TRMM satellite. The comparison between these two sensing systems involves a number of corrections that are described by Pessi et al. (2008, submitted to *Journal of Atmospheric and Oceanic Technology*). PacNet and LIS data between February 2004 and February 2007 were used for the evaluation, provided that at least 3 of the PacNet sensors were operational. The median location accuracies over the east, central, and west boxes were 13, 35, and 40 km, respectively (see Fig. 10)

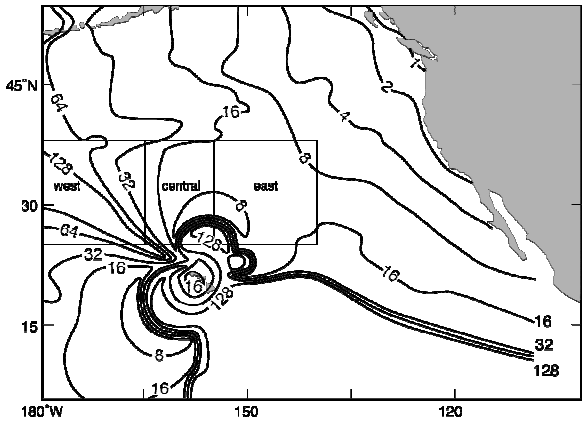

Figure 10. Modeled LA (km) of LLDN in the central Pacific with four PacNet sensors located in Alaska, Kwajalein, Lihue, and Kona. The boxes show the areas where the observed LA was assessed.

5. SUMMARY

In this paper, we have described a thorough analysis of the performance of the Vaisala Long Range Lightning Detection Network (LLDN), including PacNet. The parameters necessary for modeling the performance of PacNet were calibrated by two means. First, sensor-level performance was evaluated using the well-characterized performance of the NLDN and CLDN over a wide range of distances from a single PacNet sensor. In addition to this, LLDN detections by the NLDN and CLDN sensors were evaluated at a moderately long distance using the high-resolution PREPA network. This ground-truth detection efficiency study allowed for calibration of the detection efficiency model for daytime and nighttime conditions. The calibrated model was then applied to PacNet domain, given the PacNet sensor characteristics determined from the single PacNet sensor embedded in the NLDN. When satellite-based LIS lightning observations were used to check the detection efficiency and location accuracy in the PacNet domain, these were found to be consistent with the calibrated model estimates.

The calibration and validation of the detection efficiency model opens up the potential for quantitative detection efficiency correction of LLDN data. Preliminary demonstrations of this were shown by Pessi and Businger (2008, submitted to *Journal of Applied Meteorology and Climatology*), who examined lightning-rainfall relationships using DE-corrected lightning information, and by Demetriades and Holle (2008), who corrected lightning rates in tropical cyclones.

6. APPENDIX

This appendix presents a general detection efficiency model for lightning location systems.

The task of lightning detection begins with the electromagnetic field produced by the lightning discharge. In the case of CG lightning being detected at VLF/LF frequencies, the peak field strength (electric and/or magnetic) is roughly proportional to the peak current of the return stroke (Cummins et al., 1998b). The magnitude of the resulting field at a remote sensor location, which establishes the detectability of the signal by that sensor, is determined by three factors: (1) the attenuation of this field strength associated with normal propagation, (2) additional losses due to finite conductivity along the propagation path, and (3) imperfect (loss) ionospheric reflections. Once this attenuated signal reaches a remote sensor, it must exceed the detection threshold of the sensor, which is determined by sensor gain, threshold setting, and local noise. To obtain a location for the lightning discharge, the signal must be seen by a sufficient number of sensors, which depends on strike point location (relative to the detecting sensors), and on the applied location method (MDF, TOA, or combined).

A graphical depiction of the detection process that is amenable to direct modeling is shown in Fig. A1. The first step involves the occurrence of a CG stroke with peak current I0, selected from the probability distribution PI (the peak-current distribution). The peak electric and/or magnetic field produced by the stroke, having traveled a distance ri, then reaches sensor Si with incident signal SSi. The probability of the sensor detecting this stroke is defined by the sensor DE function, illustrated in Fig. A1. Note that there is a minimum signal strength (detection threshold) below which no events are detected, and that the maximum detectability is not reached until the signal is a bit larger than the detection threshold. Note also that as signal strength increases further, the DE decreases and eventually returns to zero when the sensor “over-ranges” and is no longer able to provide reliable information. Since each sensor that detects a specific stroke will be at a different distance, they may all have different sensor DE values for this stroke. Using the assumption that each sensor responds independently from all other sensors, these DE values are independent for each sensor i. Based on this assumption, and by defining the probability of sensor Si not detecting the event as Qi(I0) = 1-DEi(I0), then the probability of a specific combination of sensors detecting the event is simply the product of the appropriate Pi(I0) and Qi(I0) values for all sensors. For example, the probability P that a stroke with current I0 is detected by a minimum of 2 sensors of a 3 sensor network, is

$$[DE_1(I_0)*DE_2(I_0)*Q_3(I_0)] + [DE_1(I_0)*Q_2(I_0)*DE_3(I_0)] + [Q_1(I_0)*DE_2(I_0)*DE_3(I_0)] + [DE_1(I_0)*DE_2(I_0)*DE_3(I_0)].$$

Using this construct, it is possible to determine the probability of detection for any specific number of sensors in a network of arbitrary size to produce a modeled overall DE estimate for a region, the region of interest is typically broken up into a set of rectangular grid cells. For a point in the center of each cell, and for each possible peak current value, the model must determine the DE for each sensor. To determine the overall network detection efficiency for a specific peak current and grid point, one simply sums the probabilities for “N” or more sensors detecting a discharge, where N is the minimum number of sensors required by the network to locate a discharge. For networks that employ MDF in combination with TOA, N is two. For networks that employ direction finding by itself, N is 2-3, depending on the stroke location relative to the sensors locations. For networks that employ only the TOA method, N is 3-4. The overall DE is determined from the sum of DE values for each current value (I0), weighted by their probability of occurrence taken from the peak current distribution Pi.

This general parametric model has been employed over the past 15 years to estimate LLS performance. Recent validation of the model (for CG lightning detection in the U.S. involving ground-wave propagation paths) is provided in the work by Biagi et al. (2007).

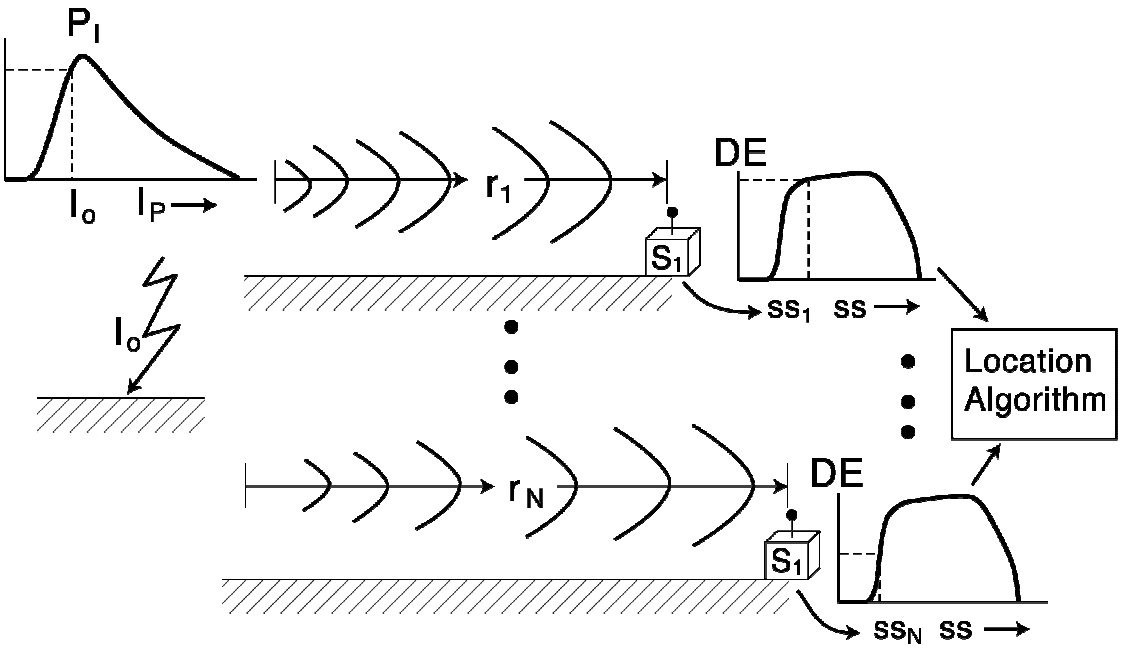

Figure A1. Simplified schematic for LLS network detection efficiency. Io is the strike peak current, P1 is the peak-current probability distribution, r1…rn are the distances between the strike and the sensors S1…Sn. SS1…SSn are the incident signals at the sensors S1…Sn. If the DE threshold is met then the signal is passed on to a central location algorithm.

7. REFERENCES

Biagi, C.J., K.L. Cummins, K.E. Kehoe, and E.P. Krider, 2007: National Lightning Detection Network (NLDN) performance in southern Arizona, Texas, and Oklahoma in 2003-2004. *J. Geophys. Res.*, **112**, doi:10.1029/2006JD007341.

Chronis, T.G., and E.N. Anagnostou, 2003: Error analysis for a long-range lightning monitoring network of ground-based receivers in Europe, *J. Geophys. Res.*, **108**(D24), 4779, doi:10.1029/2003JD003776.

Cummins K.L., E.P. Krider, and M.D. Malone, 1998a: The U.S. national lightning detection network™ and applications of cloud-to-ground lightning data by electric power utilities. *IEEE Transactions on Electromagnetic Compatibility,* **40**, No. 4, 464-480.

Cummins, K.L., M.J. Murphy, E.A. Bardo, W.L. Hiscox, R.B. Pyle, and A.E. Pifer, 1998b: A combined TOA/MDF technology upgrade of the U.S. National Lightning Detection Network. *J. Geophys. Res.*, **103**(D8), 9035-9044.

Demetriades, N.W.S. and R.L. Holle, 2008: Analysis of inner core lightning rates in 2005-2006 Atlantic and east Pacific tropical cyclones using Vaisala's Long-range Lightning Detection Network (LLDN). *3rd Conf. on Meteorological Applications of Lightning Data*. New Orleans, LA, Amer. Meteorol. Soc., paper 1.2.

Demetriades, N.W.S. and R.L. Holle, 2005: Long-range lightning applications for hurricane intensity and precipitation nowcasting. *Preprints, Conf. on Meteorological Applications of Lightning Data*. San Diego, CA, Amer. Meteorol. Soc., 9 pp (CD-ROM).

Johnson, R.L., D.E. Janota, and J.E. Hay, 1982: An operational comparison of lightning warning systems. *J. Appl. Meteorol.,* **21**, 703-707.

Kelso, J.M., 1964: *Radio ray propagation in the ionosphere*. McGraw-Hill, New York, 408 pp.

Keogh, S., E. Hibbett, J. Nash and J. Eyre, 2006: The Met Office Arrival Time Difference (ATD) system for thunderstorm detection

and lightning location. *Met Office, Numerical Weather Prediction : Forecasting Research Technical Report* No. **488**, e-mail:nwp_publications@metoffice.gov.uk

McRae, W.M., and N.R. Thomson, 2000: VLF phase and amplitude: Daytime ionospheric parameters, *J. Atmos. Sol. Terr. Phys.*, **62**(7), 609–618.

Nash, J. and Coauthors, 2005: Progress in Introducing New Technology sites for the Met Office long range lightning detection system. *Paper 2.9 WMO Technical Conference on Meteorological and Environmental Instruments and Methods of Observation (TECO-2005),* Instruments and Observing Methods Report No. **82**, WMO/TD-No. 1265.

Nickolaenko, A.P., 1995: ELF/VLF propagation measurements in the Atlantic during 1989. *J. Atmos. Sol. Terr. Phys.,* **57**, 821-834.

Orville, R.E., and G.R. Huffines, 2001: Cloud-to-Ground Lightning in the United States: NLDN Results in the First Decade, 1989–98. *Mon. Wea. Rev.*, **129**, 1179–1193.

Pessi, A., S. Businger, K.L. Cummins, N.W.S. Demetriades, M. Murphy, and A. Pifer, 2008: Development of a long-range lightning detection network for the Pacific: Construction, calibration, and performance. *J. Atmos. Ocean. Tech.*, submitted.

Rodger, C. J., S. Werner , J. B. Brundell , E. H. Lay , N. R. Thomson , R. H. Holzworth , and R. L. Dowden, 2006: Detection efficiency of the VLF World-Wide Lightning Location Network (WWLLN): initial case study. *Ann. Geophys.*, **24**, 3197–3214.

Squires. K. and S. Businger, 2008: The morphology of eyewall lightning outbreaks in two category five hurricanes. *Mon. Wea. Rev.*, in press.

Taylor, W. L., 1960: VLF attenuation for east-west and west-east daytime propagation using atmospherics. *J. Geophys. Res.*, **65**, 1933.

Thomson, N. R., 1993: Experimental daytime VLF ionospheric parameters*, J. Atmos. Terr. Phys.*, **55**, 173 – 184.

Wait, J.R., 1968: Theory of the terrestrial propagation of VLF electromagnetic waves, in *Advances in Electronics and Electronic Physics*, L. Marton, Ed., Academic Press.

Wait J. R. and Spies K. P., 1964: Characteristics of the earth-ionosphere waveguide for VLF radio waves, *NBS Tech. Note*, **300**.